A Numerical Study of Riemann Problems for the Two-Dimensional Unsteady Transonic Small Disturbance Equation

Sunčica Čanić [*] and Dragan Mirković [†]
Department of Mathematics
Iowa State University
Ames, Iowa 50011

Abstract. We study a two-parameter family of Riemann problems for the unsteady transonic small disturbance (UTSD) equation, also called the two-dimensional Burgers equation. The two parameters, a and b, which define oblique shock initial data, correspond to the slopes of the initial shock waves in the upper half-plane. For each a and b, the three constant states in the upper half-plane satisfy the Rankine-Hugoniot conditions across the shocks. This leads to a two-parameter family of *oblique shock interaction problems*.

In this paper we present a numerical study of global solution behavior for the values of a and b in a previously obtained bifurcation diagram. Our study supplements the related theoretical results and conjectures recently obtained by S. Čanić and B. L. Keyfitz. We employ a high resolution numerical method which reveals fine solution structures. Our findings confirm theoretical results and conjectures about the solution patterns, and deepen the understanding of the structure of several intricate wave interactions arising in this model.

Key words. Two-dimensional Riemann problems, unsteady transonic small disturbance equation, essentially non-oscillatory numerical scheme

AMS subject classification. Primary: 35L65, 35L67; Secondary: 35-04

1. Introduction

The results of this paper shed light on the structure of solutions of the unsteady transonic small disturbance equation (or the two-dimensional Burg-

[*]Supported by the National Science Foundation, grant DMS-9625831, and in part by the Department of Energy, grant DE-FG02-94ER25220.
[†]Supported by the Office of Naval Research, grant ONR N00014-96-1-0279

ers equation):

$$
\begin{aligned}
u_t + u u_x + v_y &= 0, \\
-v_x + u_y &= 0,
\end{aligned}
\tag{1}
$$

which was used by several authors to model weak shock reflection phenomena; see for example [2], [8], [11], [16]. We study a two-parameter family of oblique shock initial value problems for the UTSD equation with initial data given in the upper half-plane, $y \geq 0$, consisting of two shock waves, S_1 and S_2, defined by

$$S_1 \equiv x = a\, y \quad \text{and} \quad S_2 \equiv x = -b\, y,$$

where $a, b > 0$ are the two parameters in the problem. The initial discontinuities separate regions of constant states

$$
\begin{aligned}
U_0 &= (0, 0), \\
U_1 &= (1, -a), \\
U_2 &= (1 + a/b, 0).
\end{aligned}
\tag{2}
$$

The states U_0, U_1 and U_2 satisfy Rankine-Hugoniot conditions across the shock waves S_1 and S_2. The Rankine-Hugoniot conditions are given by

$$
\begin{aligned}
x_t\,[u] - \tfrac{1}{2}\,[u^2] + x_y\,[v] &= 0, \\
x_y\,[u] + [v] &= 0,
\end{aligned}
\tag{3}
$$

where $x = x(y, t)$ denotes the shock position. In addition, "no flow through the wall" boundary data is imposed along the x-axis:

$$v(x, 0) = 0. \tag{4}$$

See Figure 1. Thus, initial discontinuities will propagate as shocks. Asymptotically, for $t > 0$ and $y \to \infty$, the positions of S_1 and S_2 will approach the lines

$$
\begin{aligned}
x &= ay + s_1 t, \quad \text{where} \quad s_1 = \tfrac{1}{2} + a^2, \\
x &= -by + s_2 t, \quad \text{where} \quad s_2 = 1 + \tfrac{a}{2b} + b^2.
\end{aligned}
\tag{5}
$$

Following the terminology of Ref. [5] we call this the *oblique shock interaction problem*. Notice that because the two initial shocks are given independently, this initial problem is not that of oblique shock reflection.

The main theme of this paper is a numerical study of fine solution structures which occur in the zone of interaction of shock waves S_1 and S_2, for values of a and b in a bifurcation diagram introduced in Refs. [5] and [6].

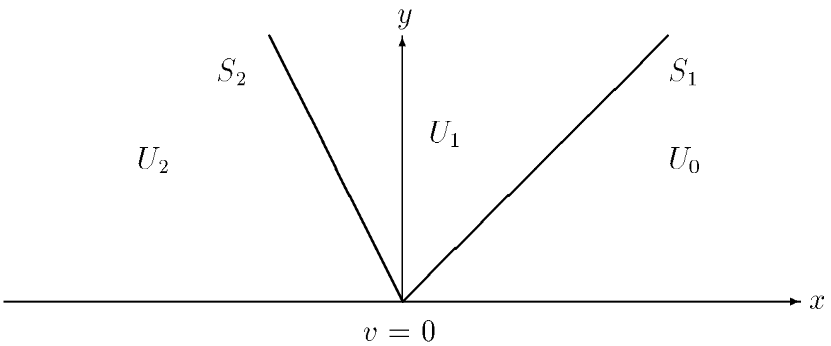

Figure 1: Riemann data

The bifurcation diagram was based on theoretical results about hyperbolic wave interactions which occur in this model, and on conjectures about interactions of shocks with the subsonic region. We employ a high resolution numerical method to resolve the intricate wave interactions.

The numerical method we implemented is described in Section 2. We used a modification of methods studied by Osher in Ref. [12] and by Osher and Sethian in Ref. [13] to approximate equation (1) in potential form.

In Section 3 we summarize the basic concepts used to obtain the bifurcation diagram in Refs. [5] and [6].

In Sections 4 to 6 we study solution patterns that comprise the bifurcation diagram.

Our findings have three important consequences.

The first is the resolution of a solution pattern arising for the parameter values in the region we call VN. For the parameter values in question, shock polar analysis for the UTSD equation does not provide a solution, and a theoretical study of the flow in the zone of interaction of waves indicates the following structure. Shock S_1 bends smoothly forming a "stem" while the shock S_2 "meets" S_1 at a point above the wall where the strength of S_2 becomes zero and the flow continuously changes from supersonic (ahead of S_2) to subsonic (behind S_2); see Figure 2. Theoretical results of Refs. [3] and [4] indicate that the horizontal component of the velocity behind the shock S_2 where its strength becomes zero, exhibits a square-root type singularity. Indeed, our numerical study of the UTSD equation enabled us to zoom in the solution and obtain a set of data for which the nonlinear least squares fit indicates the square-root type behavior predicted in Ref. [4]. Details are given in Section 5.

The second consequence of the study presented in this paper is a confirmation of the theoretical results and conjectures about the solution structures obtained in Ref. [5] for the parameter values corresponding to the regions RR and MR of the bifurcation diagram shown in Figure 4. These

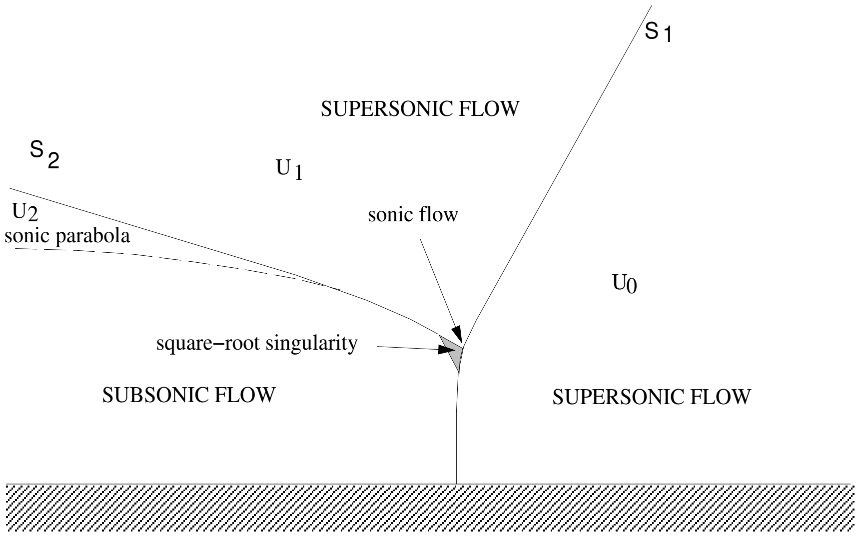

Figure 2: A sketch of the VN wave interaction pattern

are presented in Section 4.

Finally, the third is related to a resolution of the intricate wave interactions arising in the KMR and TMR regions of the bifurcation diagram. As we shall see in Section 6, for these parameter regimes numerical simulations indicate a triple shock configuration. It can be proved (see Ref. [2]) that the triple shock configuration is not possible in this model. This is the case for the full set of Euler equations and weak enough shocks as well. To resolve the triple shock paradox arising in the UTSD equation, the presence of a logarithmic singularity in the subsonic solution at the triple point was suspected. However, the work of Gamba, Rosales and Tabak in Ref. [7] shows that such a solution cannot be matched with the rest of the flow, and therefore is inadmissible. Our findings show that the state behind the shock S_2 at the triple point is, in fact, sonic; see Section 6. Thus, a quasi-one-dimensional Riemann problem takes place at the triple point. We show that this quasi-one-dimensional problem has a solution which contains a small hyperbolic region behind the point of interaction of waves. More precisely, shock polar analysis of this quasi-one-dimensional Riemann problem implies the existence of a unique local solution consisting of a shock and a thin rarefaction wave. These hyperbolic states soon become sonic and the flow changes to subsonic (see Figures 18 and 19). Our numerical simulations indicate that this solution indeed occurs. Details are given in Section 6.

2. The Numerical Method

We begin by describing the numerical method we used to study the UTSD equation. We note that our choice of a particular numerical method depended mostly on numerical evidence and the present experience in numerical approximation of conservation laws that change type. We followed the ideas given in [2], [9], [12], [13], [14], [15], and general guidance given in [10].

We solve the oblique shock interaction problem (1), (2), described in Section 1, written in potential form. Namely, since the flow is irrotational, there exists a potential, ϕ, such that $(\phi_x, \phi_y) = (u, v)$. The potential satisfies

$$\phi_{xt} + \phi_x \phi_{xx} + \phi_{yy} = 0. \tag{6}$$

Since ϕ is continuous across a shock, by fixing the value of ϕ at one point, e.g., $\phi(\infty, 0) = 0$, one recovers the initial data for (6) from (2):

$$\begin{array}{rcl} \phi_0(x,y) & = & 0, \quad x \geq a\,y, \\ \phi_1(x,y) & = & x - ay, \quad -b\,y \leq x < a\,y, \\ \phi_2(x,y) & = & \left(1 + \frac{a}{b}\right) x \quad x < -b\,y. \end{array} \tag{7}$$

Finally, the boundary data at the wall reads

$$\phi_y = 0. \tag{8}$$

To solve this problem we first integrate equation (6) with respect to x from ∞ to x (since the state ahead of the incident shock is unperturbed), to obtain

$$\phi_t + \frac{\phi_x^2}{2} + \int_\infty^x \phi_{yy}\, dx = 0.$$

Our discretization procedure is effectively divided into two steps. First, we use a semi-discrete approximation to discretize

$$\phi_t = -\frac{\phi_x^2}{2} - \int_\infty^x \phi_{yy}\, dx \tag{9}$$

with respect to the space variables. Next, a full discretization is obtained using a Runge-Kutta method for the system of ordinary differential equations obtained in the first step. The spatial domain of equation (9) is the upper half plane. Our numerical simulations are restricted to a rectangle in the upper half plane (symmetric about $x = 0$), denoted by $[x_0, x_{N_x}] \times [y_0, y_{N_y}]$, with transmission boundary conditions along the "infinite" boundary. Our computational domain is padded with two extra mesh blocks, and along the "infinite" boundary the potential ϕ is extrapolated so that the normal to the surface of ϕ remains constant. This means that the flow at the infinite boundaries will be "transmitted" through the boundary. This can be achieved everywhere where the potential is smooth. At the points where the gradient of ϕ is discontinuous (shock points) there is some reflection present, see, for example, Figure 15. However, the reflected wave is very weak and it does not contaminate the flow in the zone of interaction of waves.

The approach proposed here is similar to Brio and Hunter's from Ref. [2]. To obtain better resolution and fewer oscillations for the parameter regimes that are of interest to our study, we introduce different spatial discretization of the nonlinear term $u^2/2$, and employ transmission boundary conditions which minimize reflection from the top boundary.

Before we describe the discretization, we introduce some standard notation. For mesh sizes Δx, Δy and Δt, $\phi^n_{i,j}$ will denote a numerical approximation to the solution $\phi(x_i, y_j, t^n)$, where

$$\begin{aligned} x_i &= x_0 + i\Delta x, \quad i = 0, 1, \ldots, N_x, \\ y_j &= y_0 + j\Delta y, \quad j = 0, 1, \ldots, N_y, \\ t^n &= n\Delta t. \end{aligned}$$

Also, let $\phi_{i,j}(t)$ denote an approximation of a true solution ϕ, at (x_i, y_j) for $t \geq 0$. We denote the forward and backward difference operators in the usual way:

$$\begin{aligned} \Delta^x_\pm &= \pm(\phi_{i\pm1,j} - \phi_{i,j}), & \Delta^y_\pm &= \pm(\phi_{i,j\pm1} - \phi_{i,j}), \\ D^x_\pm &= \Delta^x_\pm / \Delta x, & D^y_\pm &= \Delta^y_\pm / \Delta x. \end{aligned}$$

We first discretize (9) with respect to the spatial variables to obtain a system of ordinary differential equations of the form

$$\frac{d\phi_{i,j}}{dt} = [F(\phi)]_{i,j}\,, \tag{10}$$

where $[F(\phi)]_{i,j}$ is a particular spatial discretization, *i.e.*, a discrete equivalent, of the nonlinear operator

$$F(\phi) = -\frac{1}{2}\phi_x^2 - \int_\infty^x \phi_{yy}\,dx.$$

Let $[N(\phi)]_{i,j}$ and $[L(\phi)]_{i,j}$ denote an approximation of the nonlinear (convection) term and the linear (diffraction) term respectively, so that

$$[F(\phi)]_{i,j} = -\frac{1}{2}[N(\phi)]_{i,j} - [L(\phi)]_{i,j}\,.$$

We describe the approximations in the following subsections.

2.1 Discretization of the Nonlinear Term

To discretize the nonlinear term we used the results from Refs. [9] and [13]. In Ref. [13] Osher and Sethian constructed ENO (Essentially Nonoscillatory) type schemes and applied them to a class of Hamilton–Jacobi equations

$$\phi_t + H(\phi_x) = 0,$$

arising in front propagation problems. High order ENO schemes are usually constructed in two steps. One begins with a first-order monotone scheme, and then builds up a higher order approximation using an ENO interpolation procedure. We follow the same steps for the spatial discretization of the nonlinear convection term

$$N(\phi) = H(\phi_x) \equiv \phi_x^2.$$

We begin with the following upwind, first order, monotone numerical flux which approximates H:

$$h(u_j^n, u_{j+1}^n) := \left[\min(u_{j+1}^n, 0)\right]^2 + \left[\max(u_j^n, 0)\right]^2.$$

This flux satisfies the numerical entropy condition:

$$\begin{aligned} h(w,z) &\leq \min_{z\leq a\leq w} H(a), \quad \text{if} \quad w \geq z, \\ h(w,z) &\geq \max_{w\leq a\leq z} H(a), \quad \text{if} \quad z \geq w. \end{aligned} \tag{11}$$

Next, a second order ENO approximation of $u = \phi_x$ can be written as

$$[\phi_x]_{i,j} = D_-^x \phi_{i,j}^n + \frac{\Delta x}{2} m\left[D_-^x D_-^x \phi_{i,j}^n, D_-^x D_+^x \phi_{i,j}^n\right], \tag{12}$$

where m is the *min-mod function*:

$$m(x,y) = \frac{1}{2}\left(\text{sgn}(x) + \text{sgn}(y)\right)\min\left(|x|, |y|\right).$$

By a result in [9], if $\phi(x)$ is piecewise C_0^∞ and if ϕ_x has at most a finite number of isolated jump discontinuities and is smooth at some point $x = x^*$, then for Δx small enough,

$$\left\{\phi_x - [\phi_x]_{i,j}\right\}_{x=x^*} = O\left((\Delta x)^2\right)$$

where $[\phi_x]_{i,j}$ is defined by (12). Moreover, the following global estimate holds:

$$\text{Total Variation}\,[\phi_x]_{i,j} \leq \text{Total Variation}\,(\phi_x) + O\left((\Delta x)^2\right).$$

Therefore, our second order approximation of the nonlinear flux is given by

$$
\begin{aligned}
[N(\phi)]_{i,j} &= \left[\max\left(D_-^x\phi_{i,j}^n + \frac{\Delta x}{2} m\left(D_-^x D_-^x \phi_{i,j}^n, D_-^x D_+^x \phi_{i,j}^n\right), 0\right)\right]^2 \\
&+ \left[\min\left(D_+^x\phi_{i,j}^n - \frac{\Delta x}{2} m\left(D_-^x D_+^x \phi_{i,j}^n, D_+^x D_+^x \phi_{i,j}^n\right), 0\right)\right]^2 .
\end{aligned}
$$

2.2 Discretization of the Linear Term

To approximate the nonlocal linear diffraction term, $L(\phi)$, we proceed as follows:

$$
\begin{aligned}
L(\phi)(x,y,t) &= \int_\infty^x \phi_{yy}(\xi,y,t)d\xi \\
&= \int_\infty^x \left[D_+^y D_-^y \phi_{i,j} + O(\Delta y^2)\right] d\xi \\
&= \frac{\Delta x}{2} D_+^y D_-^y \phi_{i,j} + \Delta x \sum_{k=i+1}^{N_x-1} D_+^y D_-^y \phi_{k,j} + O(\Delta x^2) + O(\Delta y^2).
\end{aligned}
$$

The approximation

$$
[L\phi]_{i,j} = \frac{\Delta x}{2} D_+^y D_-^y \phi_{i,j} + \Delta x \sum_{k=i+1}^{N_x-1} D_+^y D_-^y \phi_{k,j}, \tag{13}
$$

is, therefore, formally of second order because of the use of a central difference approximation for ϕ_{yy}, and the trapezoidal rule for the integration. We calculate this approximation recursively by using

$$
[L\phi]_{i,j} = [L\phi]_{i+1,j} + \frac{\Delta x}{2}\left(D_+^y D_-^y \phi_{i,j} + D_+^y D_-^y \phi_{i+1,j}\right).
$$

2.3 Time Discretization

To obtain a fully discrete scheme, second order accurate in time, we employ a second order TVD Runge-Kutta type discretization introduced by Shu and Osher in Ref. [15]:

$$
\begin{aligned}
\phi_{i,j}^{n+\frac{1}{2}} &= \phi_{i,j}^n + \Delta t\,[F(\phi^n)]_{i,j}, \\
\phi_{i,j}^{n+1} &= \frac{1}{2}\left(\phi_{i,j}^n + \phi_{i,j}^{n+\frac{1}{2}}\right) + \frac{\Delta t}{2}\left[F\left(\phi_{i,j}^{n+\frac{1}{2}}\right)\right]_{i,j},
\end{aligned}
$$

which has the same CFL condition as the first order forward Euler scheme. See Ref. [15].

We performed several tests to study convergence of the method. We ran all our examples on several levels of mesh refinement and compared our results with the exact entropy solutions in the parameter regimes for which the exact entropy solutions can be obtained. This is, for example, the case with supersonic (hyperbolic) solutions in RR and MR parameter regimes, described in detail in Section 4. Our numerical simulations indicate that this method converges to the entropy solution, and that shocks, which travel at the correct speeds, exhibit little or no spurious oscillations. See Figures 9 and 16.

Figures 9 and 16 also indicate the typical numerical shock thickness. Figure 16 provides more detail. It shows a magnified view of the mesh surface plot of the first velocity component u for a solution occurring in the MR parameter regime. The numerical results were obtained on the rectangular domain $[-23, 23]\times[0, 10]$, with the spatial discretization of 880×120 points which implies $\Delta x = 0.052, \Delta y = 0.083$. The solution is shown at time $t = 1$, after 1520 times steps at $\Delta t = 0.00066$. Figure 16 depicts a mesh surface plot of the solution on the subdomain $[-0.2, 1.4] \times [0.2, 2]$ and shows that the typical shock thickness is 4 points.

In addition to the tests mentioned above, we studied the behavior of our numerical method on a test problem of regular reflection. We started with initial data consisting of only one shock (incident shock) at an angle at which regular reflection should occur. In spite of a severe singularity in the initial data at $y = 0$, our method produced excellent results. The solution is in good agreement with the known regular reflection solution, the shocks are well resolved and they travel with the correct speeds. More details are given in the Appendix.

3. The Bifurcation Diagram

In this section we present the basic concepts used to obtain the bifurcation diagram introduced in Refs. [5] and [6], shown in Figure 4. They rely on the properties of self-similar solutions of (1).

In self similar coordinates, $\xi = x/t, \eta = y/t$, equation (1) reads

$$\begin{aligned} (u-\xi)u_\xi - \eta u_\eta + v_\eta &= 0, \\ -v_\xi + u_\eta &= 0. \end{aligned} \tag{14}$$

Equation (14) changes type across a curve

$$P_u: \quad \xi + \frac{\eta^2}{4} = u.$$

The problem is elliptic inside P_u, where the flow is subsonic, and hyperbolic outside, in the supersonic region. Linearized around a constant state $U =$

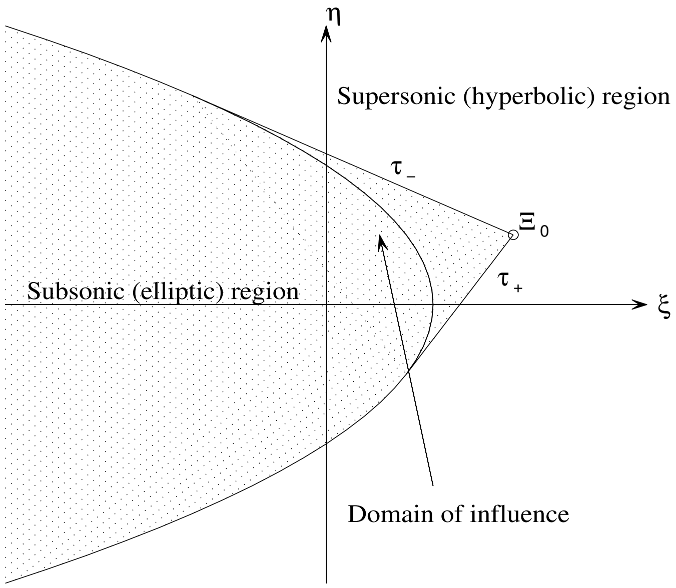

Figure 3: Domain of influence of Ξ_0

(u,v), characteristics are straight lines tangent to the parabola P_u. The *domain of influence* of a point is the union of the forward wave cone through the point and the parabola P_u. See Figure 3.

The elliptic regions corresponding to U_0, U_1 and U_2 are conveniently nested. If $\xi = \xi_S(\eta)$ denotes the shock position, the states across the shock satisfy the following Rankine-Hugoniot conditions written in self-similar coordinates:

$$\begin{aligned} \tfrac{1}{2}\,[u^2] - \xi\,[u] + \xi'\eta\,[u] - \xi'\,[v] &= 0, \\ [v] + \xi'\,[u] &= 0, \end{aligned} \tag{15}$$

where $[\cdot]$ denotes the jump in a state variable across a shock. The initial value problem (1) and (2) in self-similar coordinates becomes a Cauchy problem with data given along a space-like curve at infinity. Unlike the full set of compressible Euler equations, or the wave equation, a space-like curve at infinity for the UTSD equation is not a circle. Because the x-axis is time-like, we are not allowed to impose data at $x \to -\infty$. We can think of the Cauchy data as given along a parabola P_R, with $R \to \infty$. (More details are given in Ref. [5].) This is the reason why, using the numerical method described in the previous section, we sweep the domain from right to left, with data given in the computational domain (computational rectangle) along the upper and the right edge of the rectangle, with $v = 0$ along the wall (bottom edge).

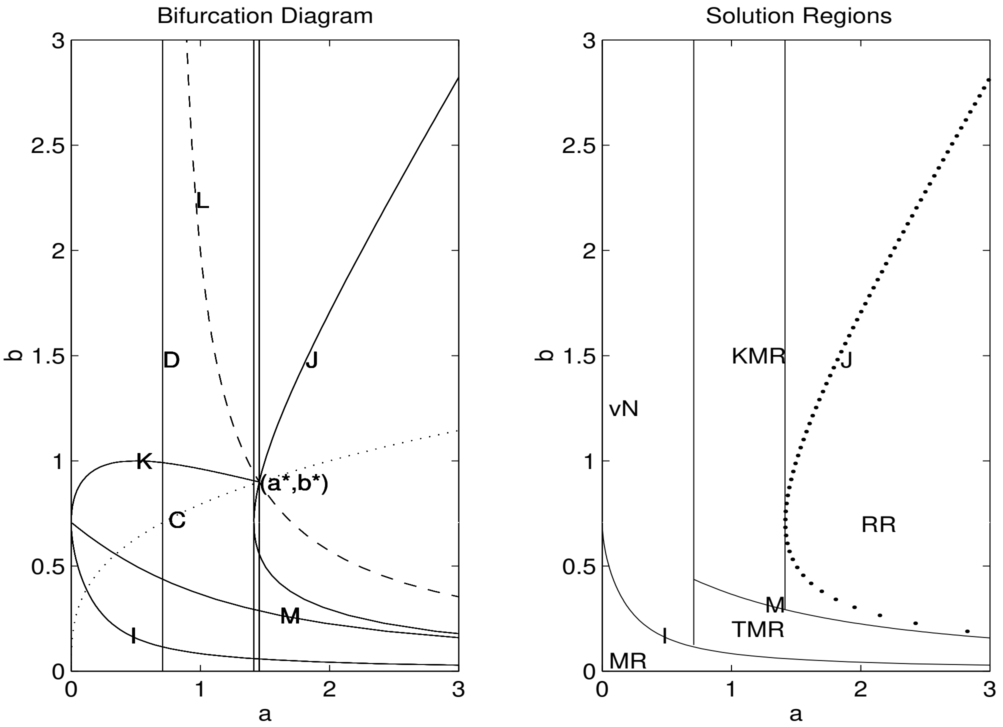

FIGURE 4: The bifurcation diagram and the solution regions

Depending on the values of a and b, shock S_2 either overtakes S_1, the shock S_1 travels faster than S_2, or S_1 and S_2 travel with the same speed, *i.e.*, $s_1 = s_2$. See equation (5). The last case corresponds to the curve J, defined below, lying in the RR region of the parameter space. The corresponding wave pattern looks like the initial shock configuration sliding along the wall with the speed $s_1 = s_2$. For other parameter values one of the following three things can happen. The two shocks can interact in the strictly hyperbolic region giving rise to new hyperbolic waves, the shock S_1 can hit the wall and generate a new wave which "joins" S_2, or, one or both shocks can first interact with the subsonic region leading to a free-boundary problem for the position of a transonic shock. Based on the type of hyperbolic wave interaction and the type of free-boundary problem that arise for different values of a and b, a bifurcation diagram, shown in Figure 4, was conjectured in Refs. [5] and [6].

A geometric description of the curves that comprise the bifurcation diagram can be summarized as follows.

Curve J**:** The curve J corresponds to the loci of points for which the two shocks, S_1 and S_2, meet at the wall leading to the "uniform RR-wave pattern". A simple calculation, requiring $s_1 = s_2$, shows:

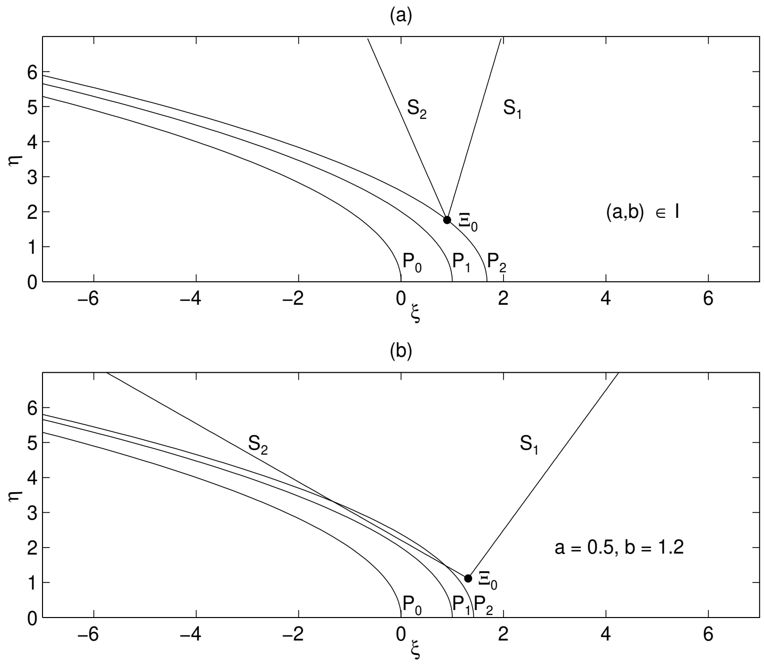

Figure 5: Geometry of shocks and the corresponding parabolas

Proposition 1 *The shocks S_1 and S_2 meet at the wall if $a = b + 1/(2b) \equiv J(b)$.*

The curves I and K: The curve $I \cup K$ is defined as the locus of points for which S_1 and S_2 intersect at the boundary of the elliptic region P_2. See Figure 5a. A calculation gives the following:

Proposition 2 $I \cup K \equiv \left\{(a,b) | a^2 + \left(2b - \frac{3}{b}\right) a + \left(\frac{1}{2b} - b\right)^2 = 0\right\}$.

The intersection of S_1 and S_2, Ξ_I, is outside P_2 if $I \cup K > 0$. This happens if a is not between the roots

$$a_{1,2} \equiv \frac{3}{2b} - b \pm \sqrt{2}\sqrt{\frac{1}{b^2} - 1} \tag{16}$$

of the quadratic defined in Proposition 2. Notice that if $b > 1$, Ξ_I is always outside P_2.

Definition 1 *We define K to be the curve*

$$\begin{aligned} a &= a_1, \quad \text{for} \quad 0 \le b \le 1, \\ a &= a_2, \quad \text{for} \quad \tfrac{1}{2} \le b \le 1. \end{aligned} \tag{17}$$

Notice that not all shock intersections in the hyperbolic region will lead to a hyperbolic wave interaction which is determined by the data at infinity. For example, Figure 5b shows that for $a = 0.5$ and $b = 1.2$ the intersection, Ξ_I, lies "beyond" P_2. Namely, before intersecting with S_1, the shock S_2 "passed through" P_2 and "emerged" on the other side of P_2 moving "backward in time". Before resolving the interaction with S_1, we need to solve a free-boundary problem for the transonic part of S_2. Therefore, the intersection $S_1 \cap S_2$ will most likely not occur at Ξ_I, but at a perturbed point $\widetilde{\Xi}_I$.

To distinguish the shock intersections that lead to hyperbolic problems determined by the data at infinity, we have the following.

Definition 2 *([5]) An admissible intersection is one that is completely determined by the data at infinity.*

Proposition 3 *All points (a, b) that lie below the curve*

$$I(b) \equiv \frac{3}{2b} - b - \sqrt{2}\sqrt{\frac{1}{2b^2} - 1} \tag{18}$$

such that $b < 1/\sqrt{2}$, have the property that $\Xi_I \equiv S_1 \cap S_2$ is an admissible intersection.

Curve D: This is the locus of points (a, b) for which shock S_1 hits the wall exactly at a point $(\xi, \eta) = (u_1, 0)$ at which P_1 intersects $\eta = 0$. A simple calculation shows that D is defined by the curve $a = 1/\sqrt{2}$. As we will see in Section 5, this curve serves as the right boundary of the VN region in the bifurcation diagram of Figure 4.
Curves $a = \sqrt{2}$ and $a = a^*$: These curves play important role in determining the boundary of the RR region where the wave pattern consists of a uniform shock S_1 and the shock S_2 (possibly perturbed), which meet at a point on the wall. For $a < \sqrt{2}$ no RR-wave pattern is possible, see Refs. [2] and [5]. For $a \le a^* \equiv \left(1 + \sqrt{5}/2\right)^{1/2}$ the state behind the (perturbed) shock S_2 cannot be hyperbolic. More details will be given in Section 4.
Curve M: Since the curve M lies in the region above I and below K, the shock S_2 intersects the parabola P_2 before intersecting S_1. If the intersection of S_1 and S_2 occurs before S_2 becomes tangent to some parabola, P_T, and starts moving "backward in time", the type of interaction between S_1 and S_2 leads to a perturbed MR-wave pattern described in Section 6. Assuming small changes from uniform flow (therefore, assuming small changes in the position of S_2 after it enters the subsonic region P_2), the upper boundary of the region in the parameter space where this configuration occurs is determined by calculating the set of points (a, b) for which the shock S_2

intersects S_1 exactly at a point of tangency to the parabola P_T. A simple calculation shows that this happens for

$$a = M(b) \equiv \frac{1}{2b} - b.$$

To study the structure of solutions that occur in different regions of the bifurcation diagram shown in Figure 4, we will have to solve a class of quasi-one-dimensional Riemann problems. Quasi-one-dimensional Riemann problems for the UTSD equation were studied in detail in Ref. [5]. We present here a summary of the techniques, and use it in later sections.

3.1 Quasi-one-dimensional Riemann Problems

The study of local solutions of quasi-one-dimensional Riemann problems arising in self-similar solutions for oblique shock initial data (2) is based on a generalization of wave-curve analysis coupled with the Lax admissibility criterion. In contrast with one-dimensional Riemann problems, the coefficients of the system (14) depend not only on the state variables, but on the physical variables as well. This means that the solution of a quasi-one-dimensional Riemann problem will depend on the position where the wave interaction takes place in the physical space. Therefore, a quasi-one-dimensional problem has data consisting of a *center* Ξ_I, and two states U_1 and U_2, given along a space-like line, L, through Ξ_I. The solution is a function

$$U(\tau) = U\left(\frac{\xi - \xi_I}{\eta - \eta_I}\right)$$

defined *downstream* from L, in a forward half-space below L. To define the *downstream wave locus* of a state U_i with respect to a fixed point Ξ_I, $D(U_i, \Xi_I)$, we first define the shock and rarefaction polars. For precise definitions see Ref. [5].

The Shock Polar For a straight line shock $\xi = \xi_I + \tau(\eta - \eta_I)$ the Rankine-Hugoniot conditions (15) imply, after eliminating $\tau = \xi'(\eta)$, that the equation for the shock polar through U_i is given by

$$\frac{[v]}{[u]} = \frac{\eta_I}{2} \pm \sqrt{\frac{\eta_I^2}{4} + \xi_I - \left(\frac{u + u_i}{2}\right)}. \tag{19}$$

If U_i is hyperbolic at Ξ_I, there are two sonic points $U_{s\pm}$ on the shock polar. At $U_{s\pm}$ the value of u equals $u_s = \eta_I^2/4 + \xi_I$. If

$$\tau_\pm(U) \equiv -\frac{\eta_I}{2} \pm \sqrt{\frac{\eta_I^2}{4} + \xi_I - u} \tag{20}$$

denote the characteristics passing through Ξ_I, then the standard Lax admissibility condition implies that $\tau = \xi'(\eta)$ must be between $\tau_+(U)$ and $\tau_+(U_i)$ for an admissible $+$-shock, and between $\tau_-(U)$ and $\tau_-(U_i)$ for an admissible $-$-shock. Transonic shocks are admissible if the state with real characteristics, U_i, is *upstream*, *i.e.*, if $u_i \leq u$. More details can be found in Ref. [5].

The Rarefaction Polar Writing system (14) in the form

$$A(U,\Xi)U_\xi + B(U,\Xi)U_\eta \equiv \left[\begin{pmatrix} u-\xi & 0 \\ 0 & -1 \end{pmatrix}\partial_\xi + \begin{pmatrix} -\eta & 1 \\ 1 & 0 \end{pmatrix}\partial_\eta\right]\begin{pmatrix} u \\ v \end{pmatrix} = 0$$

implies that a centered simple wave $U(\tau)$ satisfies

$$(A - \tau B)\,U' = 0, \tag{21}$$

where $U' = dU/d\tau$. Therefore, the null vector U' satisfies $\tau u' + v' = 0$, where $\tau = \tau_\pm(U)$, or

$$\frac{dv}{du} = \frac{\eta_I}{2} \mp \sqrt{\frac{\eta_I^2}{4} + \xi_I - u}.$$

After integrating we obtain the *rarefaction polar* through U_i, centered at Ξ_I:

$$v = v_i + \frac{\eta_I^2}{2}(u-u_i) \mp \left\{\left(\frac{\eta_I^2}{4} + \xi_I - u\right)^{3/2} - \left(\frac{\eta_I^2}{4} + \xi_I - u_i\right)^{3/2}\right\}. \tag{22}$$

Since both U and U_i must be hyperbolic at Ξ_I, the curve is defined for $u \leq u_s = \eta_I^2/4 + \xi_I$. We will denote by R^- and R^+ the branches of the rarefaction polar that correspond to the $-$ or $+$ sign, *i.e.*, to τ_- or τ_+ characteristics.

The Downstream Wave Locus The downstream wave locus of a state U_i is the set of all states U which can be joined to U_i by a shock or a rarefaction wave in which U_i is the upstream state, [5]. If U_i is hyperbolic, the downstream wave locus is the union of the loop part of the shock polar, defined for $u > u_i$, and the two branches of the rarefaction polar, defined for $u \leq u_i$. See Figure 6.

We conclude this section with a result on the existence and uniqueness of solutions of quasi-one-dimensional Riemann problems for the UTSD equation. In contrast with one dimensional Riemann problems, quasi-one-dimensional problems do not have solutions for all choices of initial data. Even when the existence is guaranteed, uniqueness of a solution may fail.

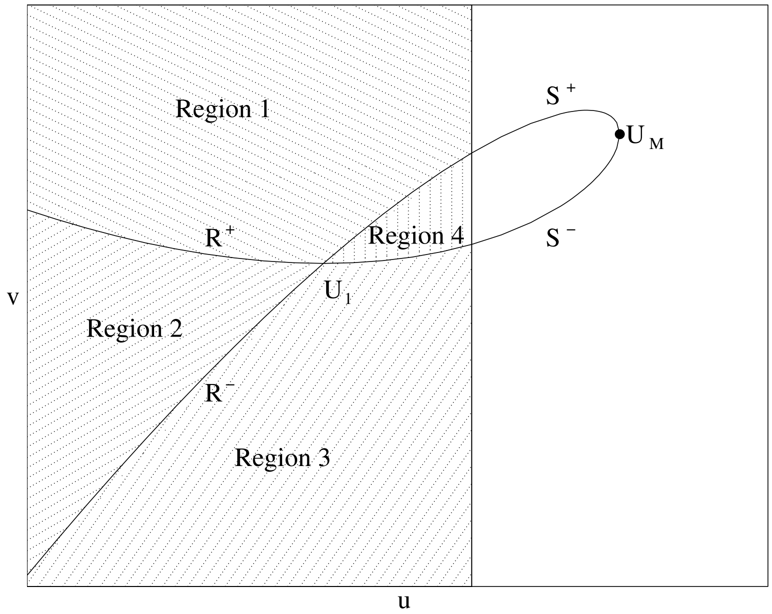

Figure 6: Downstream wave locus and solution regions of quasi-one-dimensional problems

The following theorem, proved in Ref. [5], gives a complete description of the existence and uniqueness properties of local solutions for quasi-one-dimensional Riemann problems arising in self-similar solutions of the UTSD equation.

Theorem 1 *Let (U_1, U_2, Ξ_I) be a Riemann data triple with hyperbolic states U_1 and U_2 at Ξ_I, with U_1 on the lower and U_2 on the upper half of a space-like line L through Ξ_I. Then if U_2 lies in any of the regions 1,2, or 4 in the complement of the downstream wave locus of U_1, $D(U_1, \Xi_I)$, shown in Figure 6, the Riemann problem has a unique admissible solution. If U_2 lies in region 3, the Riemann problem may have none, one or two solutions.*

4. The RR- and MR-Wave Patterns

We begin the description of the structure of solutions by first considering the cases in which quasi-one-dimensional Riemann problems arise in the strictly hyperbolic region. We present global solutions and compare the numerical simulations with the exact local solutions in the neighborhood of the point where the shock interaction takes place.

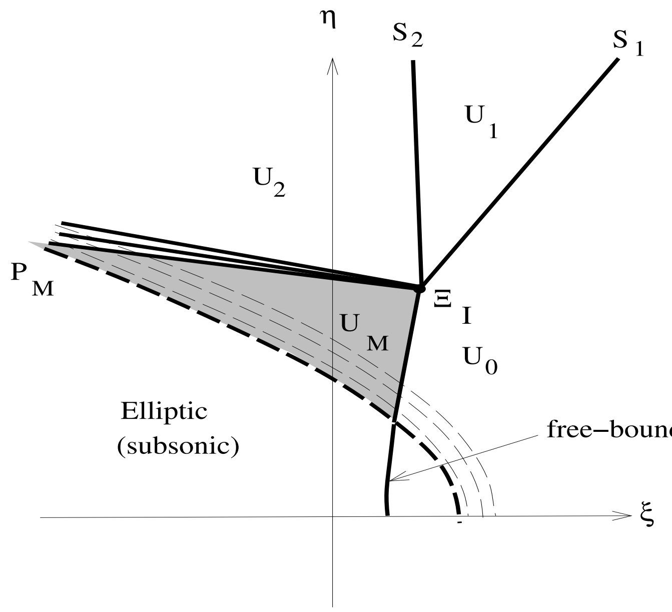

FIGURE 7: Sketch of the MR-wave pattern

4.1 THE MR-WAVE PATTERN

The region denoted by MR in the bifurcation diagram of Figure 4 is bounded by $a = 0$, $b = 0$, and by the curve $a = I(b)$, defined in the previous section. For the parameter values in this region the two shock waves, S_1 and S_2, intersect in the hyperbolic region before either of them interacts with the subsonic region. The intersection point, Ξ_I, is given by $\Xi_I = (1/2 + a/2b + ab, 1/2b + b - a)$. The solution of the corresponding wave interaction can be obtained locally, near Ξ_I, by solving a quasi-one-dimensional Riemann problem with data (U_0, U_2, Ξ_I). The following theorem, proved in Ref. [5], describes the solution.

Theorem 2 *If oblique shock data (2) given for equation (1) are such that $a \leq I(b)$, then a hyperbolic quasi-one-dimensional Riemann problem occurs at Ξ_I. Furthermore, there is a unique admissible solution which consists of a rarefaction wave and a shock.*

A sketch of the solution is shown in Figure 7. A numerical simulation is presented in Figure 8. Figure 8 shows a contour plot of v at $t = 1$ for the point $(a, b) = (0.2, 0.1) \in$ MR. The corresponding values of Δx and Δy are $\Delta x = 0.026$, $\Delta y = 0.046$. The solution was obtained after 2653 time steps. The values of v along the cross-sections 1 and 2 are shown in Figure 9. Figure 8 shows S_1 and S_2 intersecting at a point Ξ_I that lies in the

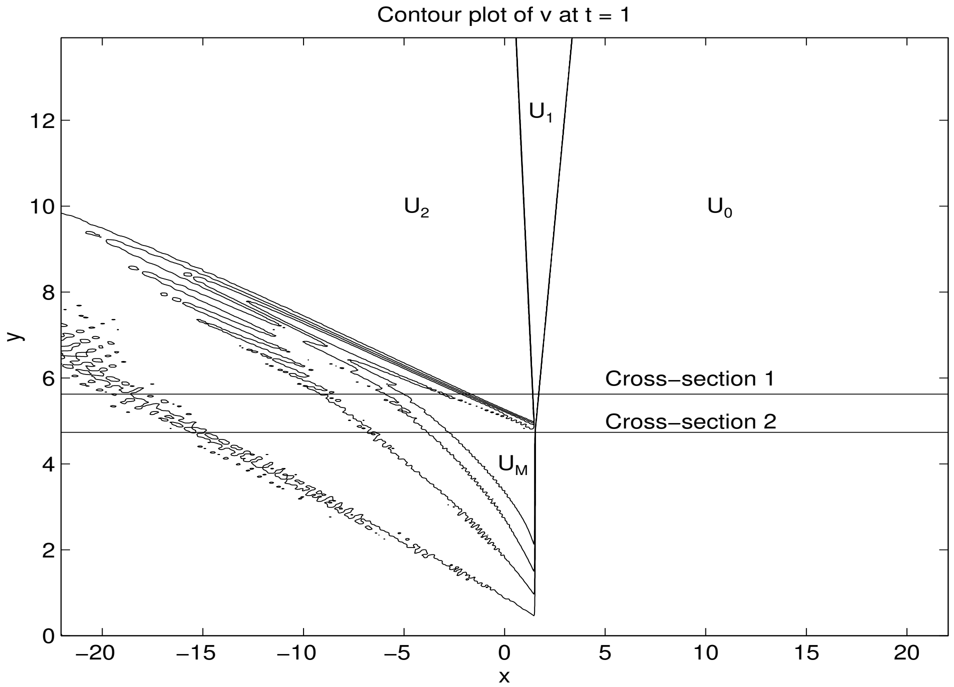

FIGURE 8: Numerical simulation of the MR-wave pattern with $\Delta x = 0.026$, $\Delta y = 0.046$ after 2653 time steps; contour plot of v at $t = 1$ for $a = 0.2, b = 0.1$. The values of v along the cross-sections 1 and 2 are shown in Figure 9.

region of supersonic (hyperbolic) flow, giving rise to new hyperbolic waves: a $+$-shock between U_0 and an intermediate state U_M, and a $-$-rarefaction wave between U_2 and U_M. The region of nonuniform flow corresponds to the subsonic region which is bounded by the sonic parabola P_{u_M}. Along cross-section 1, moving in the direction from left to right, Figure 9 shows the value of $v_0 = 0.0$, a shock from v_0 to $v_1 = -0.2$ (S_1), a shock from v_1 to $v_2 = 0.0$ (S_2), a thin rarefaction wave from v_2 to v_M, a thin region with constant state v_M, and a region of subsonic flow. Along cross-section 2, Figure 9 shows a shock from v_0 to v_M followed by the region of subsonic flow.

To compare the numerical and the exact value of U_M we solved the local hyperbolic wave interaction at Ξ_I by using the downstream loci through U_0 and U_2. The configurations of the downstream wave loci through U_0 and U_2 are given in Figure 10. The intermediate state, U_M, which lies in the intersection of the R^--branch of the rarefaction polar through U_2, and the S^+-branch of the shock polar through U_0, is given by $U_M = (2.995, -0.0129)$. The numerical value at a point which lies in the middle of the region U_M of Figure 8 reads $U_M = (2.997, -0.0125)$ which is in excellent agreement with

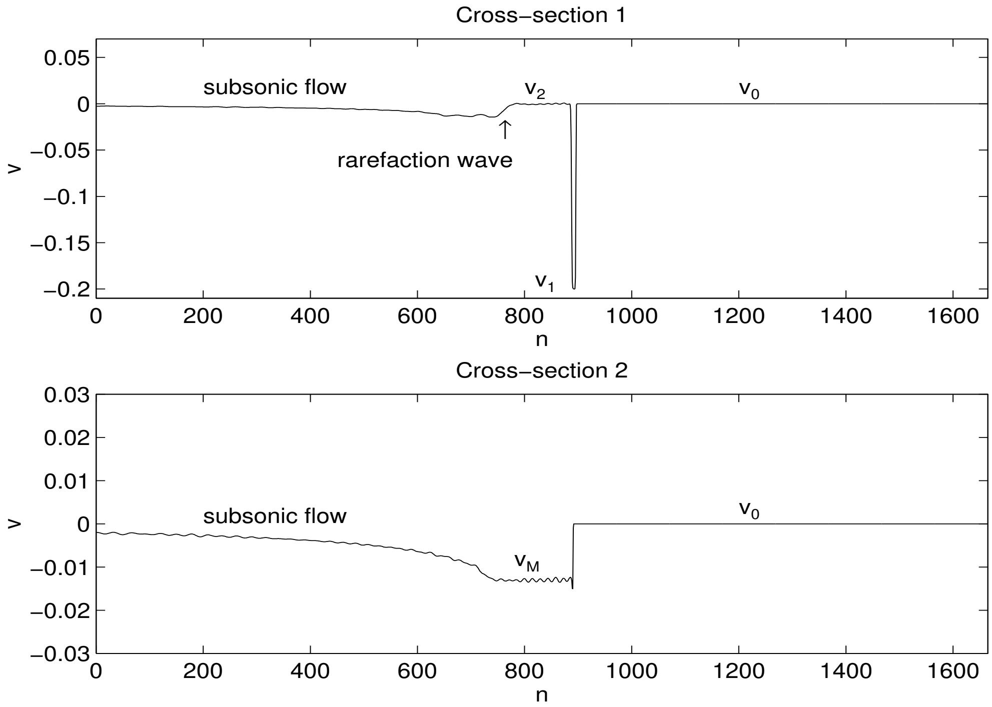

FIGURE 9: The figure shows v vs. n (mesh points) at cross-sections 1 and 2 from Figure 8.

the exact solution.

In order to complete the proof of the existence of a global solution shown in Figure 8, what needs to be done is the study of the existence of the subsonic part of the solution. This leads to a free-boundary problem for the position of the transonic shock, $\widetilde{S}_M$, between the supersonic state U_0 and the subsonic state $\widetilde{U}_M$, in the domain bounded by the wall, $\eta = 0$, by a sonic parabola P_{u_M}, and by the transonic shock $\widetilde{S}_M$ (free boundary). The natural boundary conditions associated with this problem are given by:

- no flow through the wall: $v = 0$,
- continuous flow across the sonic line: $u = u_M, v = v_M$,
- far-field conditions at $\xi = -\infty$ which guarantee $v = v_M$ along P_{u_M}, and
- two Rankine-Hugoniot conditions for the position of the transonic shock $\widetilde{S}_M$.

The existence of a solution of this problem is still open.

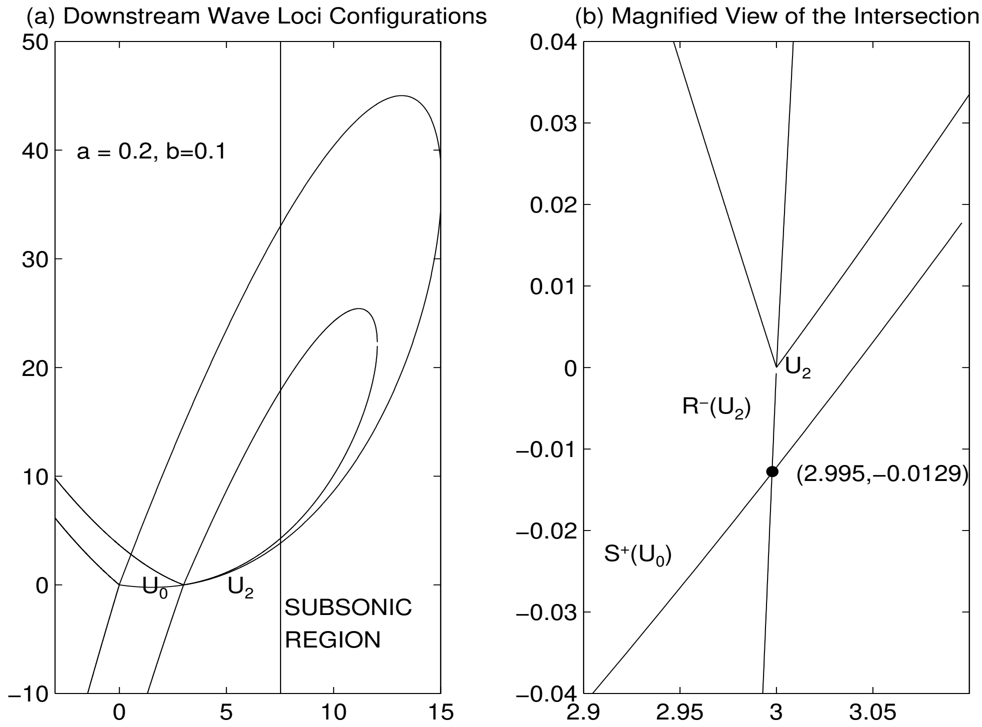

FIGURE 10: Downstream wave loci configurations for the MR-wave pattern data

4.2 THE RR-WAVE PATTERN

The RR-wave pattern denotes a solution which consists of a shock S_1 meeting with S_2 (or a perturbation of S_2, $\widetilde{S}_2$) at a point on the wall. In this model we distinguish between *uniform* RR-*wave pattern* and *nonuniform* RR-*wave pattern* or *perturbed* RR-*wave pattern*. Uniform RR-wave pattern corresponds to the case in which both the shock S_1 and the shock S_2 are straight, separating regions of uniform flow. This wave configuration occurs for the parameter values a and b for which the horizontal velocities s_1 and s_2 are equal. Proposition 1 describes the curve in the a, b-parameter space for which this occurs. We denoted this curve by J. Figure 4.2 shows our numerical simulation of uniform RR-wave pattern for $a = 1.833$ and $b = 1.5$, at time $t = 1$, obtained after 1188 time steps. The shocks move with the correct speed $s = s_1 = s_2 = 3.859$, and at $t = 1$ they meet at the point $x = 3.859$ on the wall.

Perturbed RR-wave pattern consists of a uniform shock S_1 and a curved shock $\widetilde{S}_2$ (a perturbation of S_2). As described in Ref. [5], when the uniform shock S_1 hits the wall, the shock interaction with the wall can be resolved

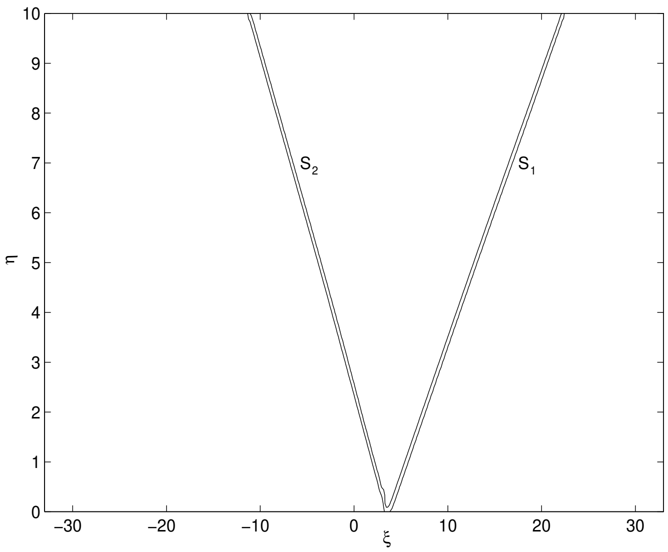

Figure 11: Numerical simulation of uniform RR-wave pattern with $\Delta x = 0.068, \Delta y = 0.083$ after 1188 time steps; contour plot of v for $a = 1.833, b = 1.5$

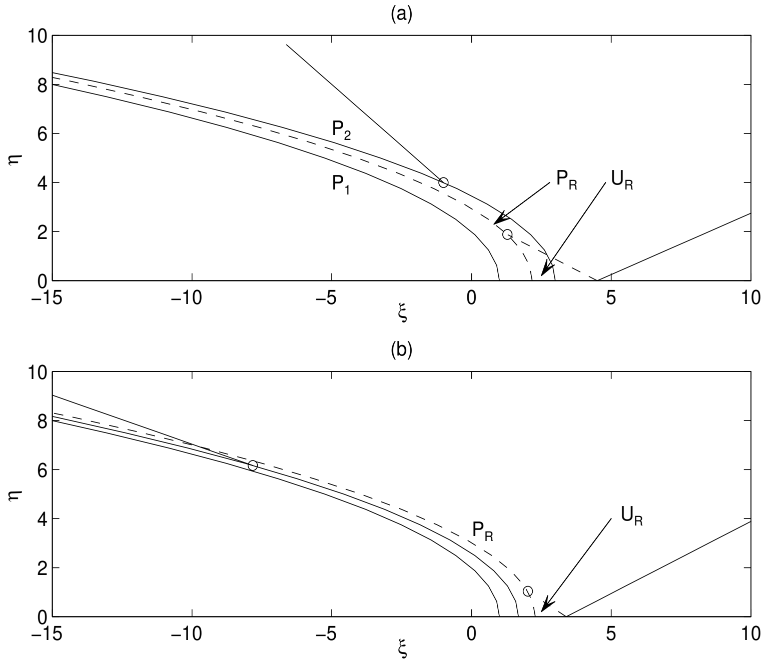

Figure 12: Geometry of shocks and sonic parabolas in perturbed RR-wave pattern. Figure 12a corresponds to $a = 2$ and $b = 1$, and Figure 12b corresponds to $a = 1.7$ and $b = 2.5$.

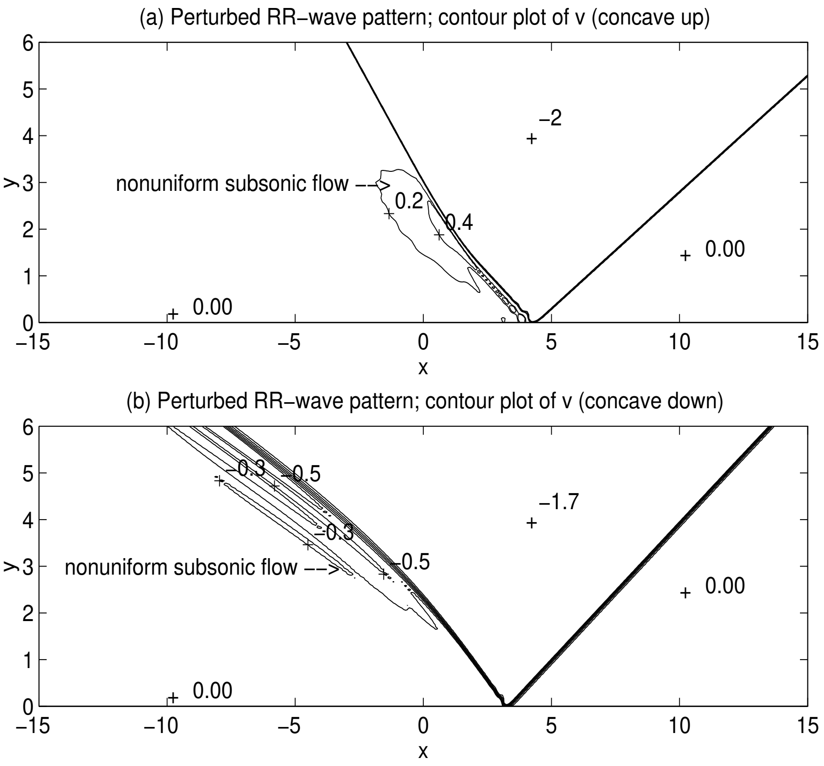

FIGURE 13: Numerical simulation of perturbed RR-wave pattern obtained with $\Delta x = 0.068$, $\Delta y = 0.083$, after 2178 time steps; contour plots of v at time $t = 1$. Figure 13a corresponds to $a = 2$ and $b = 1$, and Figure 13b corresponds to $a = 1.7$ and $b = 2.5$.

by solving a quasi-one-dimensional Riemann problem with Riemann data given by:

- the center $\Xi_A = (a^2 + 1/2, 0)$,
- a unique space-like line L (vertical line through Ξ_A), and
- the data along L: $U_1 = (1, -a)$ along the upper half of L (where $\eta > 0$), and $U_1^* = (1, a)$ on the lower half where $\eta < 0$.

Even though this is a hyperbolic problem if $a \geq 1/\sqrt{2}$, it has a solution if and only if $a \geq \sqrt{2}$. A simple calculation shows that the following proposition holds (see, for example, Ref. [5]).

Proposition 4 *The quasi-one-dimensional Riemann problem with the data triple (U_1^*, U_1, Ξ_A) has a solution if and only if $a \geq \sqrt{2}$. If $a \geq \sqrt{2}$, there* *are two solutions:*

$$\begin{array}{rcl} U_R &=& (1+a^2-a\sqrt{a^2-2},0) \\ U_F &=& (1+a^2+a\sqrt{a^2-2},0). \end{array} \tag{23}$$

The state U_F is never hyperbolic, while U_R is hyperbolic if $a \geq a^* \equiv (1+\sqrt{5}/2)^{1/2}$.

The region RR in the bifurcation diagram of Figure 4 which lies on the right of $a = \sqrt{2}$ and above the curve M, contains RR-wave pattern solutions. Some configurations of shocks and sonic parabolas for (a, b) belonging to subregions of RR are given in Figure 12. Figure 12a corresponds to $(a, b) = (2, 1)$. This point lies in the convex region of the bifurcation diagram bounded by the curve J. Figure 12b shows the geometry of shocks and sonic parabolas corresponding to $(a, b) = (1.7, 2.5)$. This point lies above the curve J, inside the region RR. (See the bifurcation diagram in Figure 4.) Notice that shock S_2 is transonic along some segment $\widetilde{S}_2$. A proof of the existence of a global solution of the free-boundary problem for the position of $\widetilde{S}_2$ is open.

Numerical simulations of perturbed RR-wave patterns are shown in Figures 13a and 13b. They were obtained with $\Delta x = 0.068$ and $\Delta y = 0.083$ after 2178 time steps. Figures 13a and 13b show contour plots of v corresponding to the parameters of Figures 12a and 12b. The contours behind the shock $\widetilde{S}_2$ in both cases show nonuniform subsonic flow. The numbers in the figures correspond to the values of v taken at the points denoted by $+$. We clearly see that the transonic shock $\widetilde{S}_2$ is concave up for $a = 2, b = 1$ (inside J), and concave down for $a = 1.7, b = 2.5$ (outside J).

5. The VN-Wave Pattern

As conjectured in Ref. [5], the VN-wave pattern occurs for the parameter values for which:

- the shock S_1 interacts with the subsonic flow before it hits the wall, *i.e.*, $\Xi_1 \equiv S_1 \cap P_1$ is admissible and $\eta > 0$. This occurs for $a < 1/\sqrt{2}$; and
- $\Xi_I \equiv S_1 \cap S_2$ is not admissible, *i.e.*, $a > I(b)$.

The corresponding geometry of shocks and sonic parabolas is given in Figure 14. To complete the global structure of the solution in the subsonic region, a free-boundary problem for the quasilinear, degenerate elliptic equation (1) needs to be solved. The free boundary consists of two parts. One

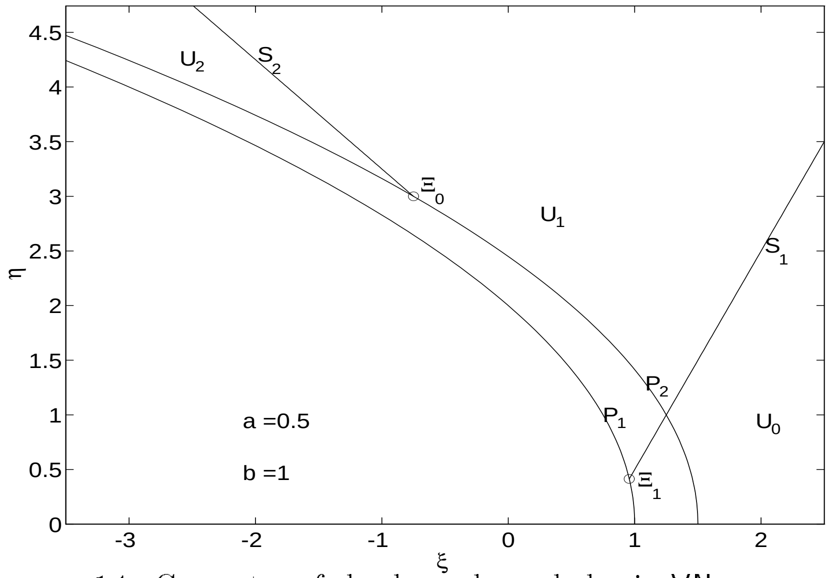

Figure 14: Geometry of shocks and parabolas in VN-wave pattern

is a continuation of the shock S_2, $\widetilde{S}_2$, where it becomes transonic, *i.e.*, from the point $\Xi_0 \equiv S_2 \cap P_2$, and the other is a continuation of S_1, $\widetilde{S}_1$, from the point Ξ_1 where S_1 becomes transonic, forming a shock stem. See Figure 14. If we introduce a new coordinate in place of ξ, so that the sonic parabolas become straight lines: $\rho = \xi + \eta^2/4$, then the shock conditions for $\widetilde{S}_1$ and $\widetilde{S}_2$ can be written as:

$$
\begin{array}{ll}
\widetilde{S}_1 \quad \ldots & \left\{ \begin{array}{lcl} \rho_s' & = & \sqrt{\rho_s - \frac{1}{2}\tilde{u}} \\ \rho_s' & = & \dfrac{\eta}{2} - \dfrac{\tilde{v}}{\tilde{u}} \end{array} \right. , \\
\widetilde{S}_2 \quad \ldots & \left\{ \begin{array}{lcl} \rho_s' & = & \sqrt{\rho_s - \frac{1}{2}(\tilde{u}+1)} \\ \rho_s' & = & \dfrac{\eta}{2} - \dfrac{\tilde{v}+a}{\tilde{u}-1} \end{array} \right. .
\end{array}
\tag{24}
$$

Here, $\rho_s = \rho_s(\eta)$ denotes the position of a transonic shock, and $\tilde{u}$ and $\tilde{v}$ are traces of the functions u and v at the subsonic side of the shock ρ_s. In Ref. [4] it was proved that if the shock stem is an increasing and convex function, *i.e.*, if $\xi_s'(\eta) \geq 0$ and $\xi_s''(\eta) \geq 0$, then $\tilde{u}$ is decreasing along $\widetilde{S}_1$. Leading order asymptotic analysis, presented in Ref. [3], implies that, if u is decreasing along $\widetilde{S}_1$, it has a square-root type singularity at the degenerate boundary where $\widetilde{S}_1$ intersects P_1. Figure 15, which shows typical contour plots of u and v in the VN-wave pattern solution indicates that the assumptions on the geometry of $\widetilde{S}_1$ are well founded. Moreover, the results in Section 5.1

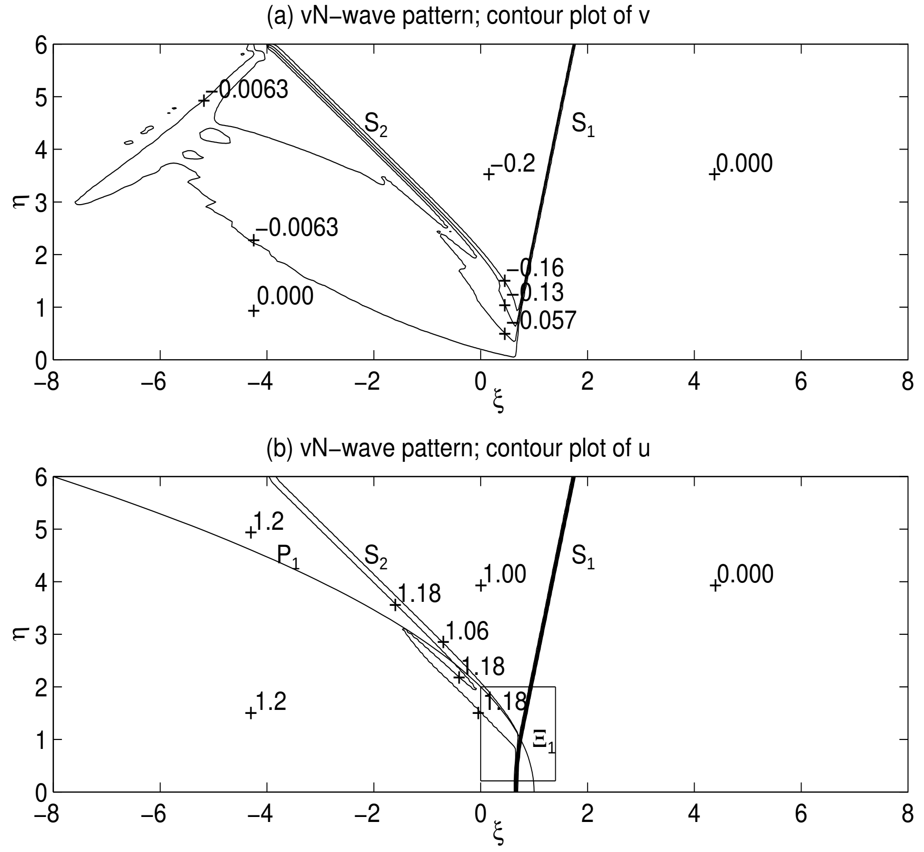

FIGURE 15: Numerical simulation of VN-wave pattern for $a = 0.2, b = 1$ with $\Delta x = 0.052$ and $\Delta y = 0.083$, after 1520 time steps; contour plots of v and u at time $t = 1$.

will show that our numerical simulations confirm the square-root behavior of u.

Regarding the structure of $\widetilde{S}_2$ we have the following observations. As for the shock stem, we first assume certain geometry of $\widetilde{S}_2$, and then use it to conclude the behavior of the subsonic solution. Namely, we would like to prove that the strength of $\widetilde{S}_2$ decreases toward $\widetilde{S}_1$ and becomes zero at the point of interaction with $\widetilde{S}_1$. The assumptions we employ are the following. If the shock $\widetilde{S}_2$ moves in the positive time-like direction, then $\rho_s' \geq 0$. This behavior is also confirmed by numerical simulations; see Figure 15. Numerical simulations also indicate the the shock $\widetilde{S}_2$ is concave down in the ξ, η-physical space. This implies $\xi_s''(\eta) \leq 0$, or, equivalently, $\rho_s''(\eta) \leq \frac{1}{2}$. Now, using these two assumptions, namely, $\rho_s' \geq 0$ and $\rho_s''(\eta) \leq \frac{1}{2}$, and the Rankine-Hugoniot conditions (24) for $\widetilde{S}_2$, we obtain that $\tilde{u}$ is decreasing from Ξ_0 towards $\widetilde{S}_1$, *i.e.*, $\tilde{u}'(\eta) \geq 0$. What is left is to show that the strength of $\widetilde{S}_2$ is zero at $\Xi_1 = S_1 \cap P_1$. This can be verified in several ways. One way is to check that the shock $\widetilde{S}_2$ between the state U_1 and a subsonic state U is tangent to the parabola P_1 at the point Ξ_1 where it intersects S_1. Namely, the following proposition holds.

Proposition 5 *A transonic shock, $\widetilde{S}_i$, between a uniform state, U_i, and a subsonic state, U, is tangent to the sonic parabola P_i at Ξ_i if and only if the strength of $\widetilde{S}_i$ is zero at Ξ_i.*

Proof: The Rankine-Hugoniot conditions for the position of a transonic shock $\widetilde{S}_i$ are given by:

$$\begin{aligned} \rho_s' &= \sqrt{\rho_s - \tfrac{1}{2}(u + u_i)}, \\ \rho_s' &= \frac{\eta}{2} - \frac{v - v_i}{u - u_i}. \end{aligned} \tag{25}$$

From the first condition we see that $\rho_s' = 0$ at a point $\Xi_i = (\rho_i, \eta_i) = (u_i, \eta_i) \in P_i$ if and only if $u = u_i$ at Ξ_i. ■

Figure 15 shows typical contour plots of v and u corresponding to the VN-wave pattern solution, obtained after 1520 time steps with $\Delta x = 0.052$ and $\Delta y = 0.083$. We added the parabola P_1 in the contour plot of u to show that the shock $\widetilde{S}_2$ is indeed tangent to P_1. We took a closer look at the behavior of u and v near Ξ_1 by studying their behavior in the boxed region shown in Figure 15b. We describe our findings in the following section.

5.1 Square-root type singularity at Ξ_1

To study local behavior of u and v near P_1 at Ξ_1 we took the traces of u and v along a straight line normal to the parabola P_1 at the point Ξ_1, shown in Figure 16. We took the data for u and v at 12 equidistant points along this line, where the first point lies above Ξ_1. Since these points do not necessarily correspond to the mesh points, we used 2-dimensional linear interpolation to calculate the corresponding values of u and v. Figure 16 shows a magnified surface plot of u at $t = 1$ above the region $[-0.2, 1.4] \times [0.2, 2]$, and the interpolated 12 values of u above the normal to the parabola P_1. The rectangles on the surface of u correspond to the mesh blocks. The precise values of u obtained at the 12 points along the normal to P_1 are shown in Figure 17. The distance from the "triple point" Ξ_1 along the normal is $\rho_1 - \rho$. To study the local behavior of u and v as functions of $\rho_1 - \rho$ we calculated a nonlinear least squares fit with functions of the form

$$z(x; C, \Lambda) = \sum_{j=1}^{m} C_j x^{\lambda_j}, \quad x \in \mathbf{R^n}, \tag{26}$$

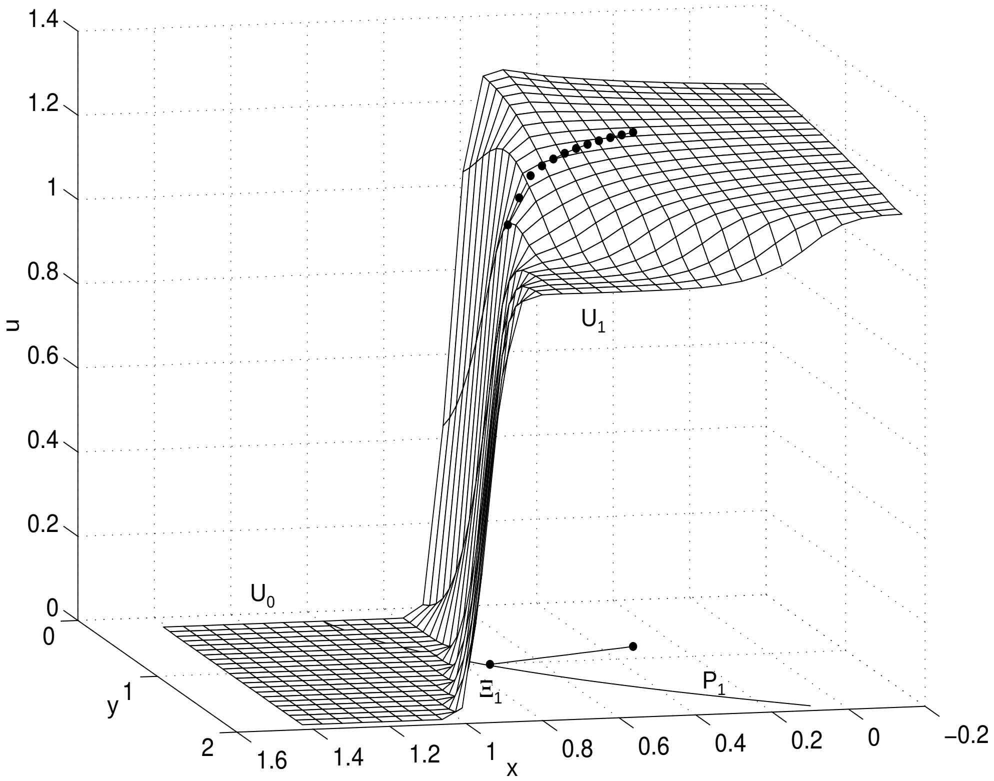

FIGURE 16: Detail of a mesh surface plot of u for $a = 0.2, b = 1$. This numerical simulation was obtained with $\Delta x = 0.052$ and $\Delta y = 0.083$ after 1520 times steps at $\Delta t = 0.00066$.

where x corresponds to $\rho_1 - \rho$, and $C = (C_1, ..., C_m)$, $\Lambda = (\lambda_1, ..., \lambda_m)$. For the horizontal velocity component u, with $m = 2$, we obtained $C = (1.0166, 0.3217)$ and $\Lambda = (0, 0.5098)$, with least square error of 0.0201. The best nonlinear fit is the function $z = 1.0166 + 0.3217x^{0.5098}$. The data and the nonlinear least squares fit are shown in Figure 17. We draw two conclusions. First, the behavior of u near the sonic point Ξ_1 can best be described as the square root of the distance from the degenerate boundary, as predicted in Ref. [4], and second, the strength of $\widetilde{S}_2$ tends to zero near the point of interaction with S_1 since the value of u near Ξ_1 approaches the value of $u_1 = 1$.

Similarly, for the vertical velocity component v, with $m = 2$, we obtained $C = (-0.1901, 0.2066)$ and $\Lambda = (0, 0.7269)$ with the least square error of 0.0065. This implies that v appears to be "smoother" near the sonic line than the function u.

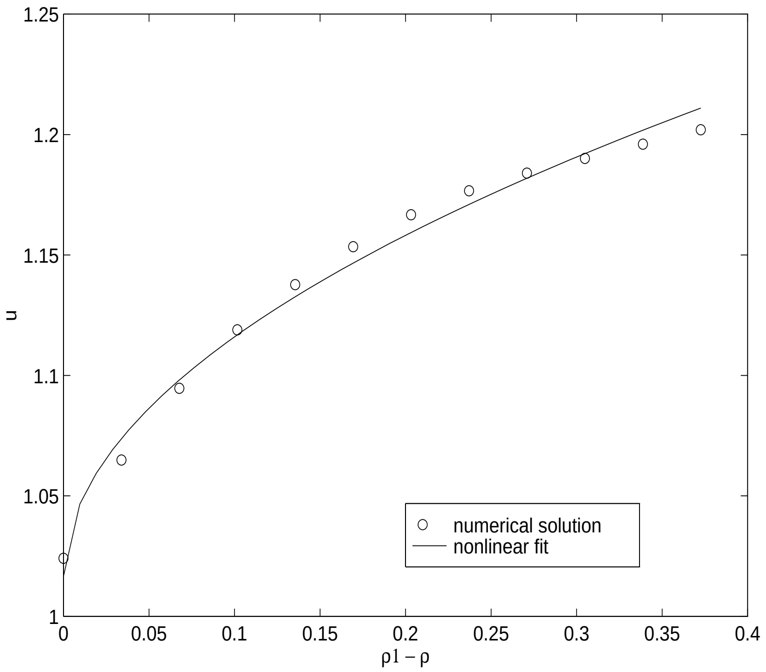

FIGURE 17: Nonlinear least squares fit of the data for the behavior of u near the sonic point Ξ_1. The data for u lies above the normal to P_1 at Ξ_1, shown in Figure 16.

6. The TMR- and KMR-Wave Patters

To complete the description of the structure of solutions for the parameter values in the bifurcation diagram shown in Figure 4, there are two regions left. They are denoted by TMR and KMR.

The region TMR is bounded from below by the curve I, on the right by the curve $a = 1/\sqrt{2}$, and from above by the curve M. The solution in this region presents a continuous transition from the solution which occurs for $(a, b) \in I$ and other types of reflection. The solution structure for $(a, b) \in I$ was first described in Ref. [5]. For completeness, we summarize the description here. The case when $(a, b) \in I$ is the limiting case in which Ξ_I is still an admissible intersection (see Definition 2). The configuration of the corresponding sonic curves and the shock waves S_1 and S_2 is shown in Figure 5a. The shock S_2 is sonic at Ξ_I and a "degenerate" hyperbolic wave interaction takes place at Ξ_I. A local solution to this degenerate wave interaction was obtained in Ref. [5]. It consists of a shock $\tilde{S}_1$ between U_0 and an intermediate state U_M, followed by a thin rarefaction wave between U_M and U_2, where the length of the characteristics in the rarefaction wave

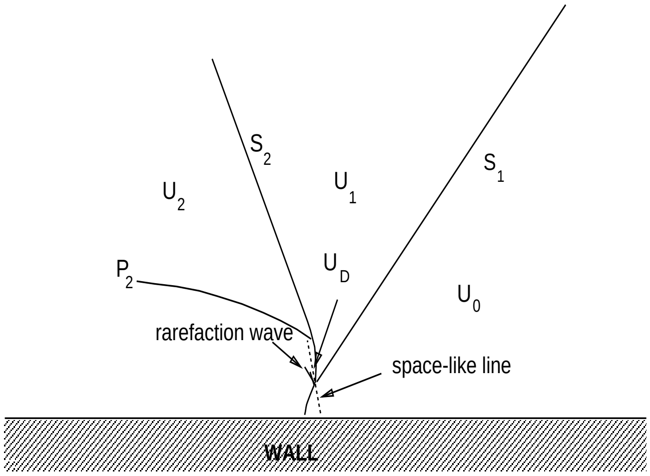

FIGURE 18: Sketch of the TMR-wave pattern

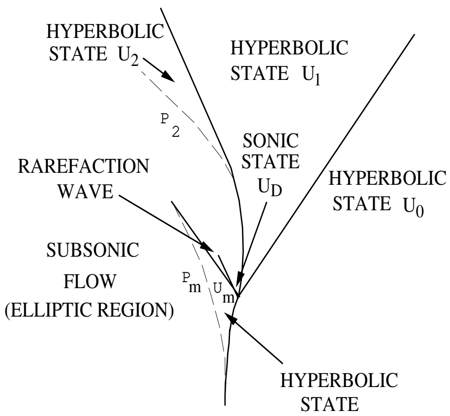

FIGURE 19: Magnified region in TMR-wave pattern near the interaction of S_1 and S_2

tends to zero as $U \to U_2$. It was proved in Ref. [5] that this solution is unique.

When $(a, b) \in$ TMR, a perturbation of this solution takes place. In this case the uniform shocks S_1 and S_2 intersect slightly inside the sonic parabola P_2, and S_2 becomes transonic from Ξ_0 to Ξ_I. The solution structure in this parameter regime has been a subject of many discussions. At a first glance the numerical pictures suggest a triple shock configuration. See Figure 20. Since the triple shock configuration cannot occur in this model, [2], the presence of a logarithmic singularity at the triple point was suspected. However, the proof presented in Ref. [7] shows that such a subsonic solution cannot be matched with the rest of the flow, and therefore, has to be discarded. The work in Ref. [5] resolves this problem in the following way. The conjecture is that the solution u decreases along the shock $\widetilde{S}_2$ and becomes sonic or supersonic at the point of interaction with S_1, giving rise to a quasi-one-dimensional Riemann problem at $\widetilde{\Xi}_I = S_1 \cap \widetilde{S}_2$. This is similar to what happens for $(a, b) \in I$. The corresponding data triple is given by $(U_0, U_D, \widetilde{\Xi}_I)$ where U_0 is the state on the right of $\widetilde{\Xi}_I$, and U_D the state on the left. The existence and uniqueness of a local solution under the assumption that the state on the left of $\widetilde{S}_2$, U_D, is sonic at $\widetilde{\Xi}_I$, was proved in Ref. [5]. Namely, the following proposition holds.

Proposition 6 *([5]) Let $a \geq \sqrt{2}$ and suppose that $\widetilde{\Xi}_I$ is any point on S_1. Then there exists a unique value U_D on $S^+(U_1, \widetilde{\Xi}_I)$ which is sonic at $\widetilde{\Xi}_I$. (The first condition means that U_D belongs to the $+$-shock branch of the downstream locus of U_1 at $\widetilde{\Xi}_I$.) Furthermore, there is a unique solution of the quasi-one-dimensional Riemann problem at $\widetilde{\Xi}_I$ with data U_0 and U_D, consisting of a shock between U_0 and and intermediate state U_m, and a rarefaction wave between U_m and U_D.*

The local solution is similar to the one occurring for $(a, b) \in I$. Figures 18 and 19, show sketches of the solution configuration. The supersonic state U_m becomes sonic at the parabola P_m and subsonic on the left of it. See Figure 19. Similarly, each state U_α in the thin rarefaction wave in which U_α changes from U_m to U_D, becomes sonic at the point where the characteristic along which U_α is constant becomes tangent to the corresponding parabola P_α, and subsonic on the left of it. Therefore, there is a small hyperbolic region near by the point where S_1 and $\widetilde{S}_2$ interact, which is "embedded" in the infinite elliptic region.

In this section we show that the state behind $\widetilde{S}_2$ at the point of interaction with S_1 is indeed sonic, and that there is a region behind $\widetilde{S}_2$ which contains points that are sonic or supersonic. In Figure 20 we show a contour plot of v corresponding to $(a, b) = (0.8, 0.15)$ which belongs to the region TMR. The values of the contours of v are taken at the positions denoted by $+$. The contour plot of v in Figure 20 shows a structure that indicates the presence of a rarefaction wave in a small hyperbolic region behind $\widetilde{S}_2$, although the structure is too small to be well resolved numerically, especially in the first velocity component u for which the jumps in the states across the shock are of greater magnitude than in the vertical velocity component v. However, to see that there is a small sonic/supersonic region behind $\widetilde{S}_2$ and the shock stem, in Figure 21 we draw the left-most contour tracing shock $\widetilde{S}_2$ and the left-most contour tracing the shock stem. We also show the boundary of the subsonic region which is numerically calculated based

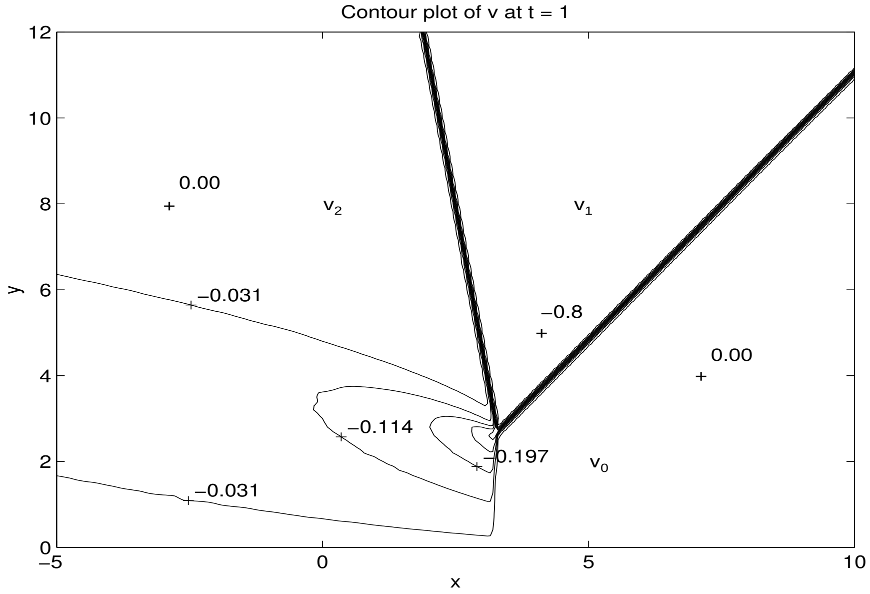

FIGURE 20: Numerical solution of TMR-wave pattern for $a = 0.8, b = 0.15$, obtained with $\Delta x = 0.05, \Delta y = 0.1$ after 1000 time steps; contour plot of v at $t = 1$.

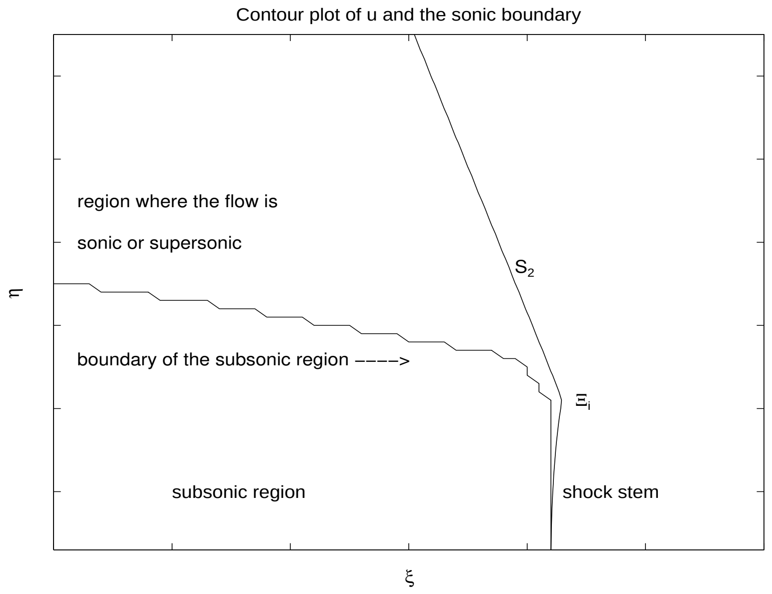

FIGURE 21: TMR-wave pattern; one contour of u and the sonic boundary

on the values of u, ξ and η. Figure 21 indicates the presence of a small sonic/supersonic region behind $\widetilde{S}_2$ and the shock stem, near Ξ_1.

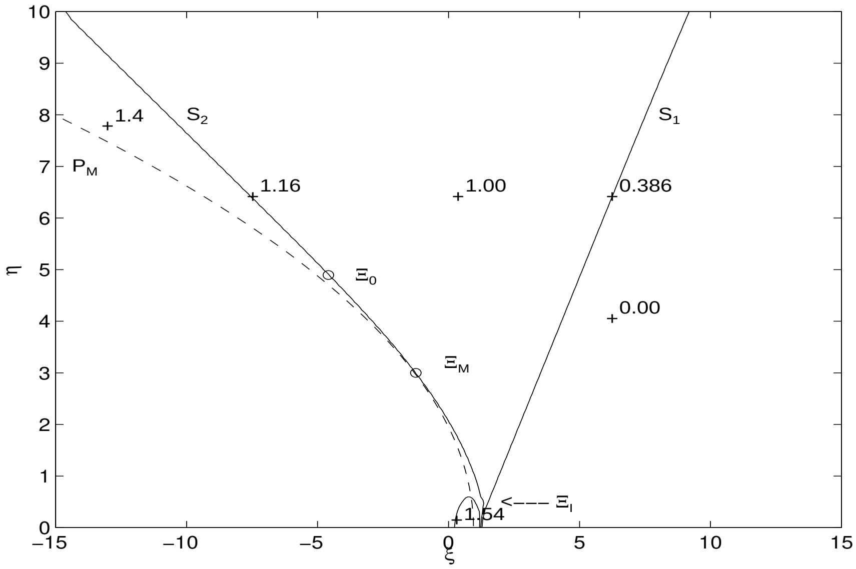

FIGURE 22: KMR-wave pattern for $a = 0.8, b = 2$ obtained with $\Delta x = 0.05, \Delta y = 0.1$ after 1000 time steps; contour plot of u with minimal number of contours.

To show that a degenerate quasi-one-dimensional Riemann problem takes place at Ξ_I, we compared the computed value of u at the "triple point", Ξ_I, and the corresponding sonic value. We have $u(\Xi_I) = 5.288$ and $u_{\text{sonic}}(\Xi_I) = 5.2153$. Considering that the point Ξ_I is in the region of high gradients where the computational error is at its worst, we conclude that the error of 7×10^{-2} is within the error bounds of the numerical method.

The structure of the KMR-wave pattern is similar to the solution occurring for the parameter values in region TMR. As conjectured in Ref. [5], the solution consists of a constant state on the left of S_2 until S_2 reaches the sonic parabola P_2. Then S_2 becomes nonuniform, reaching S_1 at a point above the wall since, by Proposition 4, it is impossible to have an RR-type solution (with S_1 straight all the way to the wall) in the region KMR. Moreover, because $a > \sqrt{2}$, the strength of the shock at the point $\widetilde{\Xi}_I$, where $\widetilde{S}_2$ meets S_1, cannot be zero. The conjecture for the solution in this case is that the shock $\widetilde{S}_2$ becomes sonic at the point where it meets S_1, and a quasi-one-dimensional Riemann problem at $\widetilde{\Xi}_I$ has a solution consisting of a shock and a rarefaction wave. The difference between this solution and the TMR-wave pattern is that the shock $\widetilde{S}_2$ becomes tangent to a certain sonic curve on its way from $\Xi_0 = S_2 \cap P_2$ to $\widetilde{\Xi}_I$. This is shown in Figure 22. The point of tangency is denoted by Ξ_M. The derivative of the position of the shock $\widetilde{S}_2$, given by the equation $\rho_s(\eta)$, changes sign at Ξ_M. The shock $\widetilde{S}_2$ moves

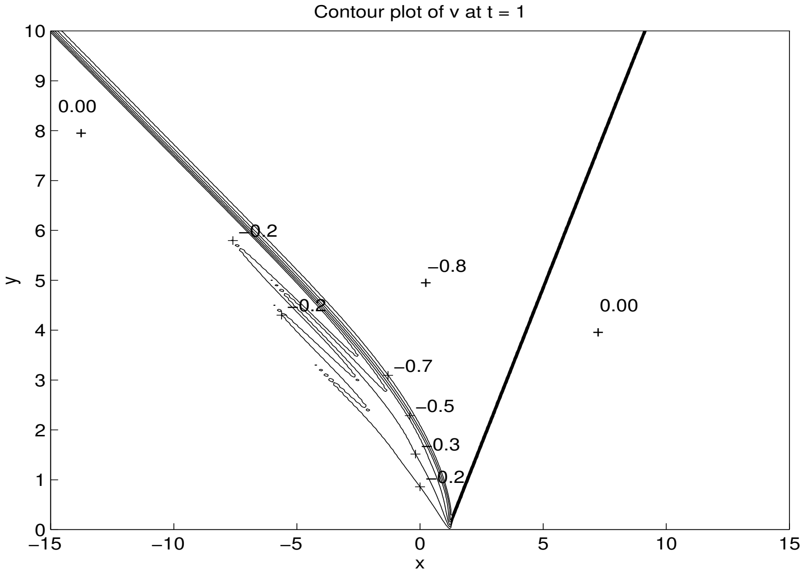

Figure 23: KMR-wave pattern for $a = 0.8, b = 2$, obtained with $\Delta x = 0.05, \Delta y = 0.1$ after 1000 time steps; contour plot of v at $t = 1$.

"backward in time" on the right of Ξ_M. Expressed in ρ, η-coordinates, the continuation of S_2, $\rho_s = \rho(\eta)$, is concave up in the neighborhood of Ξ_M, and concave down at $\widetilde{\Xi}_I$. Figure 22 shows a contour plot of u, the point Ξ_0 where S_2 intersects P_2, the parabola P_M, and the point of tangency, Ξ_M, between $\widetilde{S}_2$ and P_M. Notice how this solution interpolates between the solution occurring in the RR region (where the continuation of $\widetilde{S}_2$ can be thought of as moving "backward" in time), the solution occurring for the parameter values in the TMR region (where the structure of the local solution at Ξ_I is identical), and the solution corresponding to the VN region (where the continuation of S_2 is tangent to the parabola $P_M = P_1$ and $\Xi_M = \Xi_1$).

7. Conclusions

In this work we provided a complete description of possible wave interactions arising in a two-parameter family of oblique shock initial value problems (1) and (2) for the UTSD equation. Coupled with several theoretical results, our numerical study reveals *global* structure of solutions arising in this model.

Several questions remain open. They relate to the proofs of global existence of solutions, numerically studied in this work, and to the relevance of the solution structures studied here, to the actual problem of shock reflection.

Acknowledgement

We are grateful to Barbara L. Keyfitz for reading the manuscript and for making many helpful suggestions. We also thank the referees for their helpful comments.

The authors appreciate the hospitality of James Glimm and the Department of Applied Mathematics and Statistics at SUNY Stony Brook which both authors visited while writing the final version of the manuscript.

8. Appendix

To see how well our numerical method behaves when severe singularities are present in the initial data, we tested the method on the problem of (real) regular reflection. In contrast with the initial data consisting of two shocks S_1 and S_2, we computed our solution with a single initial shock (incident shock) at an angle which should give rise to a regular reflection wave pattern. More precisely, our initial data consists of an incident shock $x = ay$ with $a = 1.833$ between the states $U_0 = (0,0)$ and $U_1 = (1, -a)$ in the upper

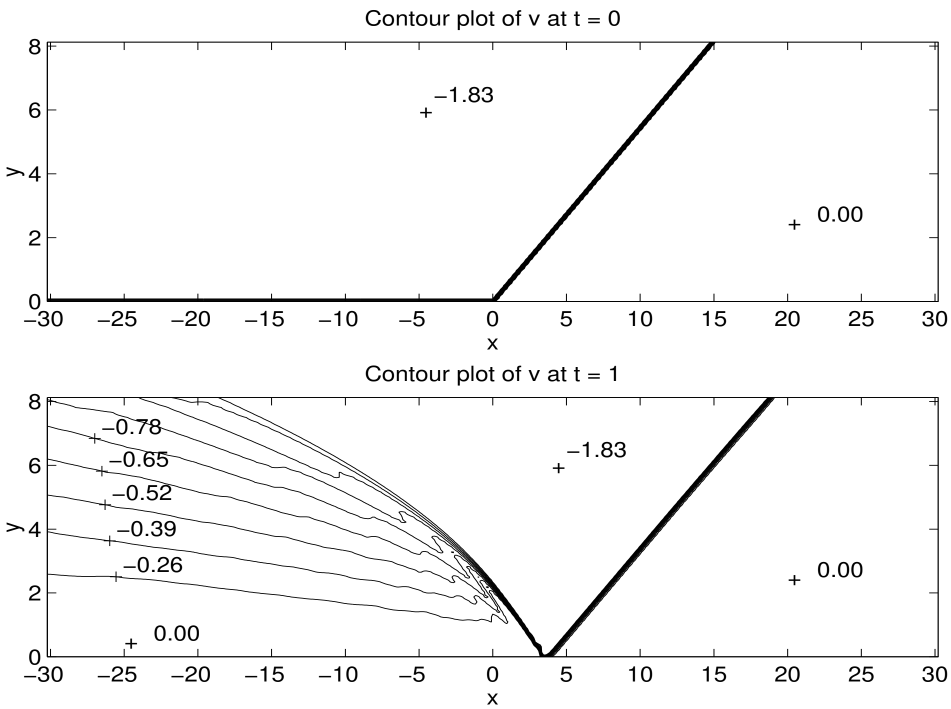

Figure 24: Numerical solution for regular reflection initial data with $\Delta x = 0.035$, $\Delta y = 0.058$, after 2115 time steps. The figures show contour plots of v at time $t = 0$ and at $t = 1$.

half plane, and "no flow through the wall" boundary condition $v = 0$. See Figure 24. Shock polar analysis implies that there are two solutions, U_R and U_L, given by

$$\begin{aligned} U_R &= (1 + a^2 - a\sqrt{a^2 - 2}, 0) \\ U_F &= (1 + a^2 + a\sqrt{a^2 - 2}, 0) \end{aligned} \tag{27}$$

which give rise to a regular reflection pattern solution (cf. Proposition 4). For the full set of Euler equations these are known as the "weak shock solution" and the "strong shock solution". For $a = 1.833$ we obtain $U_R = (2.222, 0.0)$ and $U_F = (6.497, 0.0)$. None of these solutions can be discarded on theoretical grounds. However, it is an experimental fact that the weak shock solution is the one which usually occurs (see Ref. [1]). Indeed, our numerical simulation produces the solution with the state $U_R = (2.222, 0.0)$ immediately behind the reflected wave near the point where the two shocks meet at the wall. Namely, we ran our code on the shock reflection initial data with spatial discretization $\Delta x = 0.035, \Delta y = 0.058$. We show the computed solution at time $t = 1$ obtained after 2115 time steps in Figure 24. Figure 24 shows a contour plot of v with the values along the contours indicated at the points denoted by $+$. The point where the two shocks meet at the

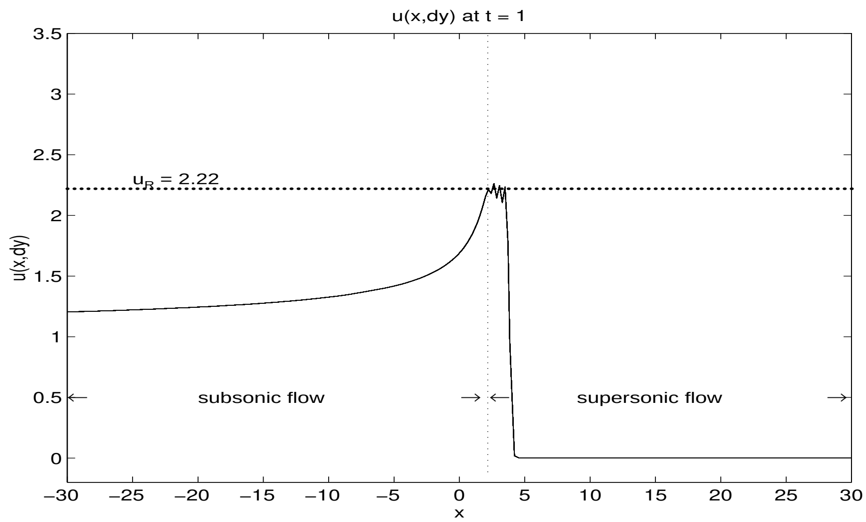

FIGURE 25: Cross-section of u at $y = dy = 0.058140$. The horizontal line $u_R = 2.22$ shows the exact value of u behind the reflected wave near the wall. The vertical line denotes the sonic boundary. It divides the plot in the region where the flow is subsonic, and therefore not necessarily uniform, and the region of supersonic flow which contains constant state u_R and a shock between u_R and $u_0 = 0$.

wall corresponds to the exact value of $x = 3.859$. To see what is the value of u behind the reflected shock close to the wall ($y = 0$), we plotted a cross-section of u at the distance $\Delta y = 0.058$ above the wall in Figure 25. Figure 25 shows a region with some oscillation around the constant state $u_R = 2.22$, a shock from u_R to $u_0 = 0$, and a region of (nonuniform) subsonic flow behind (on the left of) u_R. We conclude that our numerical results are in good agreement with the exact solution.

REFERENCES

[1] G. BEN-DOR. *Shock Wave Reflection Phenomena.* Springer-Verlag, New York, 1992.

[2] M. BRIO AND J. K. HUNTER. Mach reflection for the two dimensional Burgers equation. *Physica D*, 60:194–207, 1992.

[3] S. ČANIĆ AND B. L. KEYFITZ. An elliptic problem arising from the unsteady transonic small disturbance equation. *Journal of Differential Equations*, 125 (2):548–574, 1996.

[4] S. ČANIĆ AND B. L. KEYFITZ. Oblique shock interactions and the von Neumann paradox. In B. Sturtevant, J. E. Schepherd, and H. G. Hornung, (eds), *Shock Waves*, pages 435–440. World Scientific, Singapore, 1996.

[5] S. ČANIĆ AND B. L. KEYFITZ. Riemann problems for the two-dimensional unsteady transonic small disturbance equation. *SIAM Journal of Applied Mathematics*, 58 (2), 1998, to appear.

[6] S. ČANIĆ, B. L. KEYFITZ, AND D. H. WAGNER. A bifurcation diagram for oblique shock interactions in the unsteady transonic small disturbance equation. In J. Glimm et al., (eds), *Proceedings of the Fifth International Conference on Hyperbolic Problems: Theory, Numerics, and Applications*, pages 178–187. World Scientific, Singapore, 1996.

[7] I. GAMBA, R. R. ROSALES, AND E. TABAK. Constraints on formation of singularities for the transonic small disturbance equations. Preprint.

[8] E. HARABETIAN. Diffraction of a weak shock by a wedge. *Communications on Pure and Applied Mathematics*, XL:849–863, 1987.

[9] A. Harten, S. Osher, B. Engquist, and S. R. Chakravathy. Some results on uniformly high order accurate essentially nonoscillatory schemes. *Applied Numerical Mathematics*, 2:347–377, 1986.

[10] R. J. LeVeque. *Numerical Methods for Conservation Laws.* Birkhäuser Verlag, Basel, 1992.

[11] C. S. Morawetz. Potential theory for regular and Mach reflection of a shock at a wedge. *Communications on Pure and Applied Mathematics*, XLVII:593–624, 1994.

[12] S. Osher. Riemann solvers, the entropy condition, and difference approximations. *SIAM Journal of Numerical Analysis*, 21:217–235, 1984.

[13] S. Osher and J. A. Sethian. Fronts propagating with curvature-dependent speed: Algorithms based on Hamilton-Jacobi formulations. *Journal of Computational Physics*, 79:12–49, 1988.

[14] S. Osher and C.-W. Shu. High-order essentially nonoscillatory schemes for Hamilton–Jacobi equations. *SIAM Journal of Numerical Analysis*, 28:907–922, 1991.

[15] C.-W. Shu and S. Osher. Efficient implementation of essentially non-oscillatory shock-capturing schemes. *Journal of Computational Physics*, 77:439–471, 1988.

[16] E. G. Tabak and R. R. Rosales. Focusing of weak shock waves and the von Neumann paradox of oblique shock reflection. *Physics of Fluids A*, 6:1874–1892, 1994.